Depletion interactions effected by different variants of fd–virus

Christoph July, and Peter Lang*

Forschungszentrum Jülich, Institut für Festkörperforschung - Weiche Materie

E-mail: p.lang@fz-juelich.de

Phone: +49 (0)2461 4248. Fax: +49 (0)2461 2280

Abstract

The depletion interaction between a probe sphere and a flat wall induced by fd–virus is investigated by means of total internal reflection microscopy (TIRM). The viruses serve as a model system for mono–disperse, rod–like colloids. We find that the experimental potentials are well described by the first–order density approximation up to an fd–content of several overlap concentrations. This is in accordance with higher order density theory as confirmed by numerical calculations. Since the first order analytical description still holds for all measurements, this exemplifies that higher order terms of the theory are unimportant for our system. Comparing the potentials induced by wild–type fd to those induced by a more rigid fd variant, it can be shown that the influence of the virus stiffness is beyond our experimental resolution and plays only a negligible role for the measured depletion potentials.

Introduction

Depletion interactions between colloidal particles can govern a wide range of effects such as self-organization and induced phase transitions some examples of which are the crystallization of pro-

*To whom correspondence should be addressed

teins[1] and aggregation of colloids.[2] These interactions are therefore crucial to understanding a multitude of biologically and technologically relevant systems. Rod–like and spherical objects provide a good model system for investigating these phenomena, since they are theoretically well understood and can be grasped without the need of extensive simulations.[3] Fd-virus in particular represents an unsurpassed model for rigid and monodisperse rods[4] with high aspect ratio. The wild–type variant has a contour length of L=880 nm, a diameter D = 6.7 nm and a persistence length of L_p = 2.8 μm.[5] Because of a persistence length of about three times its own length, it is commonly regarded as long stiff rod. However, recent force-extension on M13 bactriophage (a virus virtually identical with wt–fd) and earlier laser tweezers experiments on wt-fd indicate that the persistence length might be much smaller, i. e. $L_p \approx 0.7 - 1.2\ \mu$m.[6,7] Furthermore fd-viruses are highly uniform, which is owed to their biological origin. All viruses are almost identical due to the fact that viruses clone themselves by exploiting cells of host organisms. In the case of fd those are e-coli bacteria.[8] Other forms of such biological particles are also available, for example the tobacco mosaic virus, which is stiffer than fd, but has a much lower aspect ratio with L = 300 nm and a diameter of D = 18 nm.[9] In order to approximate the ideal of completely stiff slender rods even closer while maintaining the aspect ratio, here we used a genetic mutant[10] of fd-virus, namely Y21M, in addition to wt–fd. These viruses have a persistence length of L_p=9.9 μm[10] through the altering of a protein in the virus shell.

The greater stiffness of the mutant has already been confirmed qualitatively by determining the nematic-isotropic phase transition, which occurs at lower rod densities for Y21M as compared to wt–fd. Quantitative data for the Y21M persistence length were obtained from the analysis of the viruses' twisting and bending motion as observed by video microscopy.[10] Apart from the increased persistence length, L_p, Y21M has the same properties as wt–fd.

The high degree of uniformity of fd in combination with TIRM as a measurement technique provides several experimental advantages . The force resolution of TIRM is in the fN–regime, unmatched by most other methods, p.a. AFM.[11] Further, since TIRM is a scattering technique it is next to non-invasive, which reduces the risk of data biasing by the measurement itself. Finally

the absence of polydispersity facilitates data analysis significantly[12] .

TIRM measurements of depletion potentials induced by boehmite rods[13] and fd-virus[14] have been reported earlier. In both cases satisfactory agreement between the theoretical low density prediction and the experimental data was observed. Polymeric depletants, e.g. polyethyleneoxide[15] and spherical deplentant agents, such as PNIPAM particles where also characterized by means of TIRM.[16,17] Those examples show that TIRM is a most feasible method for measuring depletion potentials close to a wall. Lin et al.[18] have reported video microscopy experiments on depletion interactions between equally sized spheres induced by wt–fd. For virus concentrations larger than five times the overlapp concentration c^* these authors find depletion potentials with contact values, that were three times smaller than those predicted by the first order density approximation. Without analyzing higher order density contributions, this discrepancy was attributed to the finite flexibility of the virus. In this article we examine the effect of flexibility at low fd-concentrations by comparing experimental data from wild–type fd and its stiffer mutant. We do not attempt to extract numbers for the persistence length of the different types of viruses. We rather compare the depletion potential they cause, to identify possible variations due to different degrees of flexibility.

Experimental

Setup, measurement principle and data evaluation

The TIR microscope was home built from standard microscopy components (Olympus), which are mounted on a X-95 rail system (Linos). The setup is sketched in Figure 1. It consists of an infinity corrected 40x Olympus SLCPlanFl objective with a focal length of f = 6.5 – 8.3 mm and a numerical aperture NA=0.55, followed by a dichroic mirror to couple in the 532 nm tweezers laser. A beam splitter equally distributes the light from the sample cell to a camera (Photometrics Cascade 1 K) and a photomultiplier tube (PMT) (Hamamatsu H7421-40). In front of the PMT a pinhole of 800 µm is used as spatial filter which, in combination with a band pass filter (λ = 633 nm), increases the signal to noise ratio to $S/N > 100$.

The sample cell is a quartz glass flow cell (QS137) from Hellma with a volume of 520 µl. Since it is completely made of glass, contaminations of the sample can be excluded. For exchanging liquids during a measurement series the cell is connected to a glass syringe with a valve by highly chemically resistive tubing (Tygon 2075 from Saint Gobain).

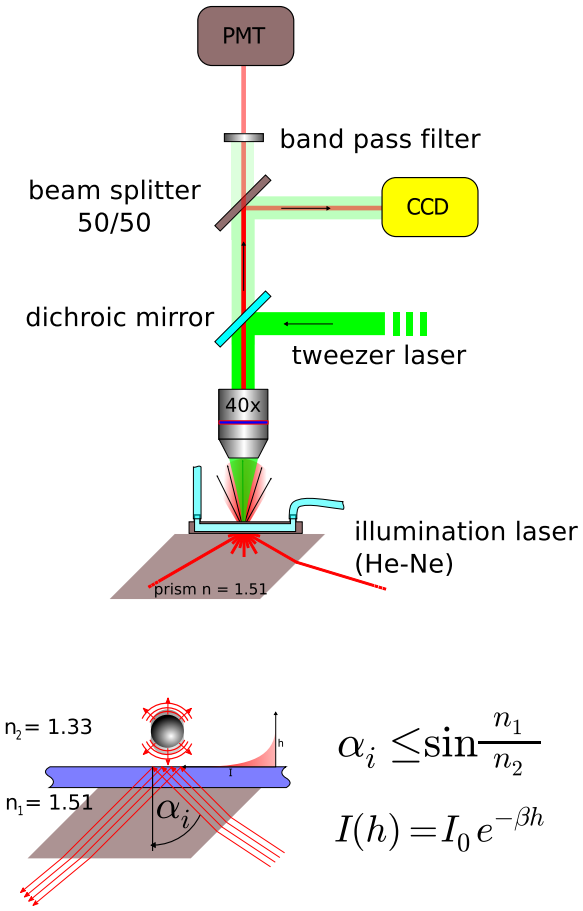

Figure 1: TIRM-setup and principle

The illumination source is a 15 mW HeNe-Laser (λ_{ill} = 632.8 nm) mounted on a goniometer, driven by a stepper motor, which allows the angle of incidence α_i to be set with high accuracy and reproducibility. A prism of BK7 glass from Edmond optics is attached to the cell to enable total reflection conditions and the creation of an evanescent wave. A thin film of immersion oil index matches possible gaps between prism and cell. An angle $\alpha_i = 65.29°$ is chosen for the experiments, which yields a penetration depth of the evanescent field intensity β^{-1}= 150 nm.

In the course of an experiment a spherical probe particle is observed, which floats at an average elevation in the range of 100 nm above the reflecting interface and which is illuminated by the evanescent field. In a typical experimental situation the interaction potential between the particle and the wall can be regarded as the superposition of an electrostatic repulsion and a gravitational attraction contribution. To keep the particle in the field of view of the microscope, it is laterally trapped by the optical tweezers. The particle is confined only in two dimensions parallel to the interface, due to the low numerical aperture of the objective. The resulting light pressure is an additional contribution to the particle's potential. Driven by Brownian motion, the particle changes elevations h, randomly, thereby sampling the potential well it's in. A change in elevation directly converts into a change in scattering intensity due to the evanescent nature of the illumination as suggested by Eq. 1. For the given experimental parameters, i. e. low penetration depth and p–polarization of the incident beam, the illumination profile can be sufficiently well described by an exponential[19,20]

$$I(h) = I_0 \exp(-\beta h) \tag{1}$$

with

$$\beta = \frac{4\pi}{\lambda_{ill}} \sqrt{(n_1 \sin \alpha_i)^2 - n_2^2}. \tag{2}$$

Here, the refractive index $n_1 = 1.51$ is that of the glass cell, while n_2 is the refractive index of the liquid, usually 1.33 for aqueous solutions. The intensity I_0 signifies the scattered intensity at zero elevation and is usually determined by adding enough salt (NaCl) to the solution to screen all electrostatic interactions and thereby allowing the particle to sediment. The knowledge of I_0 is required to enable normalization of elevations to absolute scale.

Taking advantage of the fact that the particle performs its motion according to Boltzmann statistics, the probability density, $p(h)$, of finding the particle at an elevation h can be written as,

$$p(h) = A \exp\left(\frac{-\phi_{tot}(h)}{k_B T}\right) \tag{3}$$

where ϕ_{tot} is the total sphere–wall interaction potential. Following the analysis of Prieve[21] it is presumed that the probability of observing a given intensity is equal to the probability to finding the particle at the corresponding elevation, i. e. $p(h)dh = p(I)dI$. Together with Eq. 1 this leads to,

$$p(h) = -\beta p(I)I(h). \tag{4}$$

The probability density $p(I)$ is determined experimentally, assuming that the histogram of measured intensities $N(I)$, converges to $p(I)$ for small enough bins and a sufficiently large number of events. Dividing the resulting probability density of heights $p(h)$ by $p(h_0)$ we obtain,

$$\Delta\phi(h) = \ln\left(\frac{N_{max}I_{max}}{N(I)I}\right). \tag{5}$$

Here N_{max} is the number of counts in the histogram maximum, I_{max} is the corresponding intensity, $\Delta\phi(h) = \phi(h) - \phi(h_0)$ and $\phi(h_0)$ is an arbitrarily defined potential minimum value located at h_0. Up to this point no specification of the sphere–wall potential's functional form has been made. The only constraint of the method is, that the measured probe particle has to be in thermodynamic equilibrium.

The accuracy of a potential measurements is dependent on several experimental factors. There are systematic uncertainties such as finding I_0, finding the maximum of the histogram, imperfection of probing spheres, variation of the composition of the solution. Moreover simple statistical errors such as the noise of the PMT, noise of the illumination laser and the tweezer laser contribute to the total error. Even taking this into account TIRM is a very sensitive, if not the most sensitive measurement technique available at the moment, to probe potentials of colloidal particle. A conservative estimate of the errors yields an energy resolution of 0.1 kT and a spacial resolution of about 5 nm (the statistical error on the spatial resoltion is only 1 nm). With no viruses present a potential is correctly described by the superposition of an electrostatic repulsion in the Debye–Hückel approximation, a gravitational part and a contribution due to the light pressure of the optical

tweezers, as $\phi_{ref}(h) = A\exp(-\kappa h) + F_{G,app}h$, where we defined an effective force, which drives the particle to the wall as $F_{G,app} = mg + \frac{P}{c}$. Here A is the amplitude of the electrostatic repulsion, κ^{-1} is the Debye screening length, m is the buoyancy corrected particle mass, g is the acceleration of gravity, P is the tweezers-power absorbed or reflected by the particle, and c is the speed of light. In the presence of the virus, the resulting depletion potential has to be added such that the total potential is than expressed as $\phi_{tot}(h) = \phi_{ref}(h) + \phi_{dep}(h)$ with,

$$\frac{\phi_{dep}(h)}{kT} = \begin{cases} \frac{c_{rod}N_A\pi}{3M_{rod}} L_{rod}^2 R_{sphere}\left(1 - \frac{h}{L_{rod}}\right)^3 & \text{for } h \leq L_{rod} \\ 0 & \text{for } h > L_{rod} \end{cases} \tag{6}$$

where we used the first order density approximation to describe the depletion potential.[3] The rod concentration is given by c_{rod} in units of mass per volume, N_A is Avogadro's number, M_{rod} and L_{rod} are the virus' molar mass and length, respectively, and R_{sphere} is the radius of the probe sphere.

Fitting the model function of 6 to a measured potential profile requires the introduction of an additional constant $\tilde{\phi}_{dep}(h) = \phi_{dep}(h) - \phi_0$. This is necessary, since it is not possible to measure absolute potentials, as can be seen from 5. There the value $\phi(h_0)$ is always arbitrary. In the present case, the parameter ϕ_0 represents an experimental offset, which is used to ensure that the experimental depletion potentials go to zero at $h \to L_{rod}$. Were it possible to measure up to separation distances larger than 880 nm, in that range ϕ_0 would be the constant but arbitrary difference between the actual and the reference potential.

Concerning the expression for the depletion it can be seen, it does not contain any parameter reflecting a finite flexibility of the rod, since it was devised for rigid particles. The simplest way to account for deviations from this model would be to introduce an effective quantity in the elevation independent pre–factor of Eq. 6. For the quantitative analysis of our experimental data we adhered to the following protocol. In the first step we determined the values of the parameters A, $F_{G,app}$ and κ by non linear least squares fitting the expression for ϕ_{ref} to the data, which were obtained from a situation where no virus was present in the system. These values were then kept fixed during the fitting to the data measured at finite virus concentrations. Thus, according to the modified version

$\tilde{\phi}_{dep}(h)$ of Eq. 6, ϕ_0 should be the only adjustable parameter. However, to allow for possible discrepancies between the data and the model function, we also allowed the virus concentration to float freely in the fitting procedure.

Sample preparation

Both fd–virus variants were grown in our group, following standard procedures described elsewhere.[8,22] The viruses were then transferred to a 2 mMol TRIS-HCl buffer (pH = 8.2) with 15 % ethanol by centrifuging them at 108,800 G for 8 hours five times, exchanging the solvent each time. The buffer was prepared with highly purified water with a resistivity of (ρ =18 MΩcm) and a total organic carbon content of less than 2 ppb which was mixed with ethanol (Aldrich 99.6 vol%) of high purity. The ethanol was added to the pure buffer before setting the pH to suppress bacteria growth during the experiments. The concentrations of the fd stock solutions were determined by UV-Vis-Spectroscopy with an accuracy better than 1 % using Lambert-Beer's law at λ_{ext} = 269 nm with α_{ext} = 3.84 cm^2/mg.[22] For the measurements the stock solution was diluted to the required concentrations. The glass cells were thoroughly cleaned by immersion in a mixture of 1:1 H_2O_2 (30 vol%) and H_2SO_4 (99 vol%) for over one hour. Afterwards the cells were rinsed with ultra pure water (ρ =18 MΩcm) and blown dry with dried N_2. This procedure delivered very clean surfaces of the sample cells free of any residual contamination. Syringes and tubing were cleaned by sonicating them successively in acetone, ethanol and pure water for approximately half an hour, each step.

TIRM measurements

As a first step in all experiments a very small amount of polystyrene spheres (*Thermo Scientific*) was mixed with the TRIS-buffer also used for the fd viruses. This sphere solution was inserted into the cell with a glass syringe. After having the cell filled, a suitable sphere was trapped with the optical tweezers. On this sphere a measurement with the PMT was performed, taking 500000 intensity values with a sampling rate of 500 Hz. The power of the tweezers was adjusted beforehand

to a level at which the particle was safely trapped, but the apparent weight force was low enough, to allow the sphere to sample a broad range of elevations, i. e. $F_{G,app} \approx 50$ fN.

During the exchange of the solvent with the virus suspensions of different concentrations the tweezers power was increased to a level of $F_{tweezer} \approx 1$ pN, where the solvent could safely be exchanged via the syringe without losing the particle. The cell was gently flushed with about 10 ml of the new solution to make sure that there is no unwanted dilution or mixing. This procedure was repeated until the potentials at all desired concentrations were measured. Once the measurement series had been completed the intensity scattered by the sticking sphere I_0 was recorded. For this purpose a 0.1 M NaCl solution was pumped into the cell to completely screen electrostatic interactions and thereby allow the particle to sediment.

Numerical calculation

To validate the use of the first order density approximation for the analysis of our data, we performed numerical calculations of the depletion potentials according to Mao et al.[23] The results are displayed in Figure 2 where we plot depletion potentials induced by perfect rods versus elevations for different rod concentrations. The symbols were calculated with Eq. 6 using $L_{rod} = 880$ nm, $R_{sphere} = 1.5$ μm, $M_{rod} = 1.64 \times 10^7$ g/mol. With these parameter the rods' overlap concentration $c^* = 6M_{rod}/\pi L_{rod} N_A = 0.076$ mg/ml. The full lines represent second order density calculations, which have to be performed by multidimensional numerical integration.

Third order contributions which are also discussed by Mao et al. have no significant influence at concentrations below several tens of c^* and are negligible compared to first and second order contributions. The curves in Figure 2 show that up to ten times the overlap concentration there is only a discrepancy of a few percent between first and second order calculations. This shows that the first order approximation yields sufficiently accurate results in the concentration range we were exploring experimentally, i. e. $c \leq 0.25$ mg/ml.

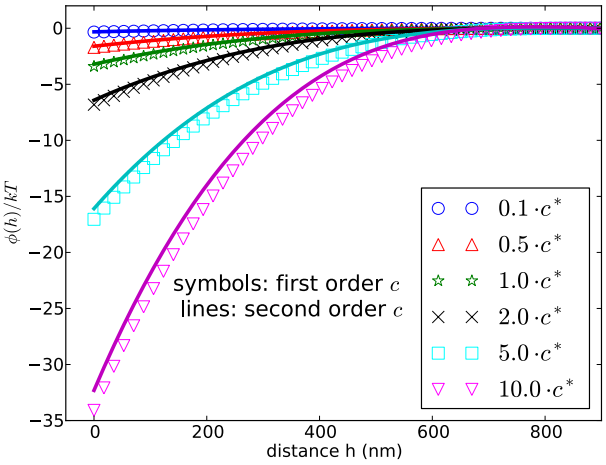

Figure 2: Numerical calculation of depletion interactions acting between a flat wall and a sphere with $R_{sphere} = 1.5$ μm, induced by rods with $L_{rod} = 880$ nm at various rod concentrations.

Results and Discussion

Measurements of the depletion potentials induced by wild type fd-virus on a $R = 1.5$ µm probe sphere are shown in Figure 3. The symbols represent experimental data and the full lines are non–linear least squares fits, which were obtained as described in the section on data interpretation. The fit of the reference potential ϕ_{ref} to the data measured in the absence of fd is obtained for an apparent weight force of $F_{G,app}$ = 51 fN and an amplitude of the electrostatic repulsion of A=559 kT.

It is obvious from Figure 3 that perfect agreement between experimental data and the model function is achieved without changing the effective virus concentration from the fd–content which was determined spectroscopically. This is a strong indication that the finite flexibility of wt–fd does not have a significant effect on the induced depletion potential. To exclude the possibility that this finding might be a coincidental artifact of the data analysis procedure, we performed measurements using the Y21M as the rod species, which is a mutant of fd–virus with a persistence length that is about $4-5$ times higher than that of the wt–fd. The resulting potentials are shown in Figure 4, where experimental data are displayed together with the best fitting model curves. In this case the best fit of ϕ_{ref} to the experimental data measured in the absence of the virus is produced by an

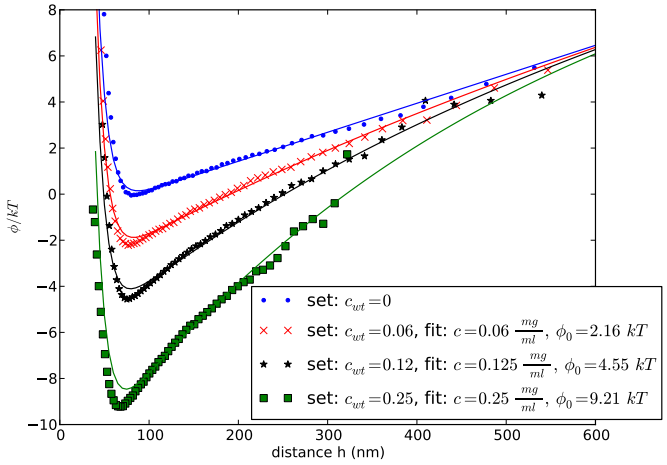

Figure 3: Measured potentials between a flat glass wall and a polystyrene sphere with R=1.5 µm for various concentrations of wild type fd–virus. Symbols represent measured data while solid lines show the fits based on $\phi_{tot}(h)$.

apparent weight force $F_{G,app}$ = 84 fN and an amplitude of the electrostatic repulsion of A=213 kT. Also here we did not find any significant deviation of the fitted effective virus concentration from the preset value.

Minor deviations between the absolute potential values of the two sets of experiments are attributed to several reasons. First, different spheres will experience different gravitational forces, caused by variations of the spheres' radii and/or mass densities. Second, the amplitude of the electrostatic repulsion varies among different spheres, because they may have different radii and/or surface charge densities. Third, the Debye screening length may change slightly in the course of an experiment due to CO_2 adsorption into the solvent. Finally, the amplitude of the depletion potential is proportional to the sphere radius and might thus vary between two series of experiments. To visualize these effects, we calculated the depletion potentials by subtracting the reference potential from the experimental total potentials obtained in the presence of the virus. The resulting data were normalized to the nominal contact value of the depletion potential $\phi_{contact}(h)/kT = c_{fit}\pi N_a R_{sphere} L_{rod}^2/3M_{rod}$ as shown in Figure 5. In this representation the depletion potentials from both types of virus fall nicely on top of each other in the range of elevations 70 nm < h < 300 nm. Only one of the curves has outliers at large separation distances. This

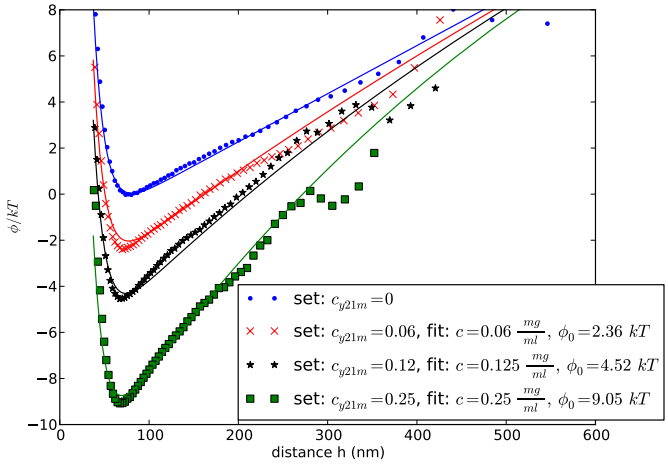

Figure 4: Measured potentials between a flat glass wall and a polystyrene sphere with R=1.5 µm for various concentrations of Y21M–virus. Symbols represent measured data while solid lines show the fits based on $\phi_{tot}(h)$.

is certainly caused by a non–identified artifact, and not by an intrinsic property of the depletant particles. Outside the specified range of elevations, $\Delta\phi \geq 3k_BT$ for the lowest virus concentration and $\Delta\phi \geq 10k_BT$ for $c_{rod} = 0.25$ mg/mL. Accordingly, the statistics of data sampling is reduced for $h < 70$ nm and $h < 300$ nm and the subtraction of the reference potential will yield unreliable potential values.

Although the normalized depletion potentials shown in Figure 5 fall on top of each other within experimental accuracy, there is still one weak point in comparing the data this way, because the experiments were performed using different spheres. We therefore run one showcase experiment, in which we first determined the reference potential, then we replaced the buffer by a wt–type fd–solution with a concentration of $c = 0.24$ mg/mL, measured the total potential, replaced the wt–virus by Y21M and measured the total potential again. Finally, we flushed the cell with 0.1 Mol/l NaCl solution to make the sphere sediment and measured I_0. By this procedure, we made sure, that we measured the two total potentials under identical conditions. After subtraction of the reference potential we obtained the two depletion potentials shown in Figure 6, together with the zero order density approximation. In addition, error bars are included in this figure, which were left out in the other figures for clarity reasons. It is apparent, that the errors are minor around the most

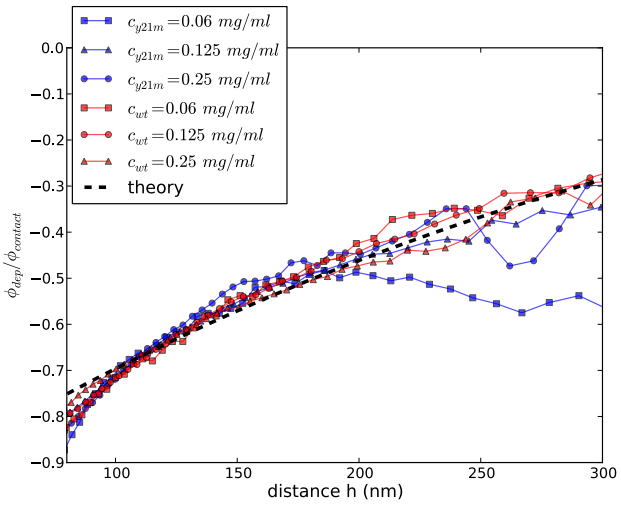

Figure 5: Depletion potentials normalized to their contact value $\phi_{contact}$ for different Y21M and wilde–type concentration (R = 1.5 µm spheres). The dashed line gives the theoretical prediction. All data curves nicely fall on top each other with a small variation around the theory curve

probable distance, even with a very conservative error estimate as it was done here. In the elevation range, where the subtraction yields statistically reliable results, we observe next to no difference between the three curves. Comparing the data points to the theoretical prediction a slight deviation is visible. This may have different possible reasons. As before non perfect referencing might influence the pure depletion potential. Furthermore data points at higher separation distances are less reliable due to decreased statistics. Nevertheless we may safely conclude that the different flexibility of wt–fd and Y21M has no measurable effect on the on the depletion potential these rods induce between a sphere and a flat wall as far as measured here. Otherwise there should be a discernible discrepancy between the two measurements, irrespective of whether they agree with the prediction or not. This observation is in line with an estimate of the depletion potential contact value, based on the bent rod model.[6] With the commonly quoted value of the wt–fd persistence length, $L_p \approx 2.5\ \mu$m, this model yields a contact value which is at maximum five percent smaller than that of a perfectly stiff rod at fixed contour length.

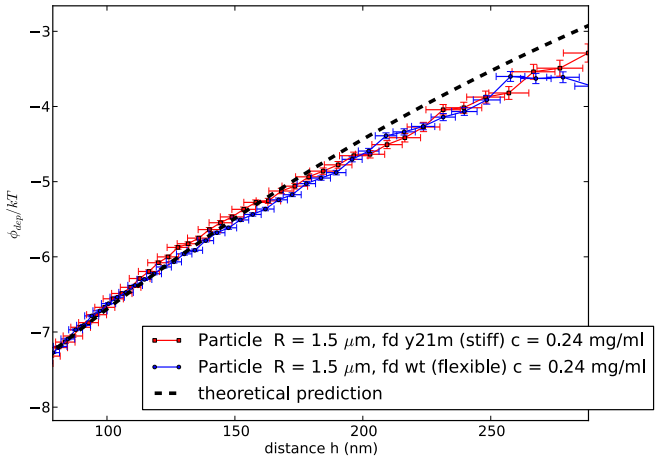

Figure 6: Direct comparision between the two virus variants. Measurements performed on one and the same sphere in one spot, keeping all experimental influences constant. There is no visible difference between the two fd-species in terms of depletion interaction. Here the theoretical prediction for the set concentration is given as a dashed line.

Conclusion

We performed TIRM–measurements of the depletion potential between spherical probe particles and a wall, which are induced by rod-shaped co–solutes. As depletants we used two different types of mono-disperse virus particles, namely wild–type fd–virus and a mutant, Y21M. Both rods have the same molar mass and rod length, but the mutant has a persistence length which is by a factor four to five larger than that of the wild type virus. The scope of this contribution was to investigate the effect of the rod's flexibility on the depletion potential it exerts. Numerical calculations and measurements prove that the analytical first order density treatment according to Mao et al. is sufficient to describe the depletion interaction correctly up to a rod content of about $3c^*$. For the two virus species probed it has been shown that flexibility doesn't have a measurable impact on the depletion interaction. This indicates that wild type fd-virus is a suitable model system for stiff rods, despite the debate about the actual value of its persistence length. In the present study we could investigate only two degrees of flexibility. A thorough investigation with different rods showing a broader variety of stiffness is desirable. It would be especially interesting to determine the ratio of contour length to persistence length at which an influence of the flexibility on the depletion

potential sets in. These investigations will become possible in the near future when a broader range of fd–mutants will be available.[24]

Acknowledgement

We thank Z. Dogic for the gift of the altered Y21M virus stock, P. Lettinga and K. Selinghoff for their help with the virus preparation. The authors acknowledge financial support from the EU through FP7, project Nanodirect (Grant No NMP4-SL-2008-213948).

Supporting Information Available

TIRM data on depletion behaviour of fd virus at various concentrations

This material is available free of charge via the Internet at `http://pubs.acs.org`.

References

(1) Gögelein, C. Ph.D. thesis, Heinrich-Heine-Universität-Düsseldorf, 2008.

(2) Neu, B.; Meiselman, H. Biophy. Jour. **2002**, 83, 2482–2490.

(3) Mao, Y.; Cates, M. E.; Lekkerkerker, H. N. W. Phys. Rev. Lett. **1995**, 75, 4548–4551.

(4) Tang, J.; Fraden, S. Liquid Crystals **1994**, 19, 459–467.

(5) L. A. Day, S. A. R., C. J. Marzee; Casadevall, A. Ann. Rev. Biophys. **1988**, 17, 509–539.

(6) Lau, A. W. C.; Lin, K.-H.; Yodh, A. G. Phys. Rev. E **2002**, 66, 020401.

(7) Khalil, A. S.; Ferrer, J. M.; Brau, R. R.; Kottmann, S. T.; Noren, C. J.; Lang, M. J.; Belcher, A. M. Proceedings of the National Academy of Sciences **2007**, 104, 4892–4897.

(8) D.A.Marvin,; Hohn, B. Bact. Rev. **1969**, 53, 172–2009.

(9) Klug, A.; Caspar, D. Adv. in Virus Research **1960**, 7, 225.

(10) Barry, E.; Beller, D.; Dogic, Z. Soft Matter **2009**, 5, 2563–2570.

(11) Kleshchanok, D.; Tuinier, R.; Lang, P. R. J. Phys.: Con. Matt. **2008**, 20, –.

(12) Lang, P. R. J. Chem. Phys. **2007**, 127, –.

(13) Laurent Helden, P. L., Gijsje H. Koenderink; Bechinger, C. Langmuir **2004**, 20, 5662–5665.

(14) P. Holmqvist, D. K.; Lang, P. Eur. J. Phys. E **2008**, 26, 177–182.

(15) Rudhardt, D.; Bechinger, C.; Leiderer, P. Phys. Rev. Lett. **1998**, 81, 1330–1333.

(16) Xing, X.; Li, Z.; Ngai, T. Macromolecules **2009**, 42, 7271–7273.

(17) Fernandes, G. E.; Beltran-Villegas, D. J.; Bevan, M. A. Langmuir **2008**, 24, 10776–10785.

(18) Lin, K.-h.; Crocker, J. C.; Zeri, A. C.; Yodh, A. G. Phys. Rev. Lett. **2001**, 87, 088301.

(19) Helden, L.; Eremina, E.; Riefler, N.; Hertlein, C.; Bechinger, C.; Eremin, Y.; Wriedt, T. Appl. Opt. **2006**, 45, 7299–7308.

(20) Riefler, N.; Eremina, E.; Hertlein, C.; Helden, L.; Eremin, Y.; Wriedt, T.; Bechinger, C. Journal of Quantitative Spectroscopy and Radiative Transfer **2007**, 106, 464 – 474, IX Conference on Electromagnetic and Light Scattering by Non-Spherical Particles.

(21) Prieve, D. Adv.Coll. Interf. Sci. **1999**, 82, 93–125.

(22) Purdy, K. R.; Fraden, S. Phys. Rev. E **2004**, 70, 061703.

(23) Mao, Y.; Cates, M.; Lekkerkerker, H. J. Chem. Phys. **1997**, 106, 3721–3729.

(24) Dogic, Z. Private Communication.

Graphical TOC Entry